

Fabrication and Test of a Diamond-turned Mirror Suitable for a Spaceborne Photometric Heliospheric Imager

Andrew Buffington^{*a}, Kirk G. Bach^b, Bernhard W. Bach^b, Erich K. Bach^b, Mario M. Bisi^a,
P. Paul Hick^{a,c}, Bernard V. Jackson^a, and Peter D. Klupar^d

^a Center for Astrophysics and Space Sciences, University of California, San Diego,
9500 Gilman Drive #0424, La Jolla, CA 92093-0424 USA;

^b Bach Research Corp., 2200 Central Ave., Suite D, Boulder CO 80301 USA;

^c San Diego Supercomputer Center, University of California, San Diego,
9500 Gilman Drive #0505, La Jolla, CA 92093-0505 USA;

^d NASA/Ames Research Center, Moffett Field, CA 94035 USA

ABSTRACT

We have fabricated a diamond-turned low-mass version of a toroidal mirror which is a key element for a spaceborne visible-light heliospheric imager. This mirror's virtual image of roughly a hemisphere of sky is viewed by a conventional photometric camera. The optical system views close to the edge of an external protective baffle and does not protrude from the protected volume. The sky-brightness dynamic range and background-light rejection requires minimal wide-angle scattering from the mirror surface. We describe the manufacturing process for this mirror, and present preliminary laboratory measurements of its wide-angle scattering characteristics.

Keywords: Very wide-angle optics, diamond-turned mirror, scattered-light measurements

1. INTRODUCTION

The Solar Mass Ejection Imager (SMEI)¹ has been providing precision photometric all-sky maps since its launch early in 2003². These SMEI maps, when the roughly 100× background of starlight and zodiacal light are properly removed, consist mostly of sunlight which has been Thomson scattered from heliospheric electrons. Time series of these subtracted maps have tracked coronal mass ejections (CMEs) from Sun to Earth^{3,4}, and have demonstrated the potential of such instruments to forecast Earth-directed CMEs well in advance of their arrival^{4,5}. Over its more-than-six-year lifetime, SMEI has also observed considerable unexpected aurorae above its 840 km altitude⁶, comet-tail motions induced by the passing solar wind⁷⁻⁹, and changes in the Gegenschein brightness¹⁰. Moreover, the background-subtracted SMEI data, when input to the University of California, San Diego (UCSD) three-dimensional (3D) reconstruction process, provide 3D heliospheric-electron density and velocity volumes over much of the inner heliosphere¹¹⁻¹³; direct measurements by *in-situ* spaceborne instruments have confirmed results from this 3D reconstruction method^{13,14}.

Although SMEI continues to provide high-quality near-all-sky photometric data, it is appropriate at this time to consider future directions for this type of instrument. The need for precision measurements of heliospheric electrons is likely to continue, both to provide forecast capability for “space weather”, and to further deepen our understanding of the physical processes affecting the solar wind between Sun and Earth. SMEI is the best design we know for this type of instrument in low Earth orbit; however SMEI data often suffer significant interference with particle-hits from the South Atlantic Anomaly and the auroral ovals, together with the auroral light itself. A SMEI follow-on would offer improved coverage and performance if located further from the Earth, for example in deep space at one of the Lagrange points, or as a “free flyer”. A practical instrument design for reaching such deep-space locations requires a considerable reduction in mass compared with the three SMEI cameras, and has been developed¹⁵⁻¹⁷ (and proposed) for a variety of deep-space missions^{18,19}.

* E-Mail: abuffington@ucsd.edu; phone: 1 858 534 6630; Fax: 1 858 534 0177

A key element in this design is a slightly curved corral which provides many decades of stray-light reduction¹⁷ within its protected volume, even when light incident from bright objects is only a few degrees below its plane, and thus outside of its “field of regard” (the hemisphere above the corral). A second key element is a hemispherical imager which views down to the edge of the corral but does not protrude above its plane¹⁶. This article describes the manufacturing of a low-mass mirror suitable for such a hemispherical imager, and preliminary measurements of the stray-light scattering of its diamond-turned surface.

1.1 A low-mass hemispheric imager design

Figure 1 presents a schematic diagram of an imager such as described earlier. For its simplest heliospheric-observing application, the Sun and other bright objects such as illuminated spacecraft appendages must be placed at least a few degrees below the plane of the imager, and the optical system situated within views the hemisphere above the corral. Normal “fisheye” lenses tend to protrude above the plane of the corral, or if placed further down within the darkened volume, are unable to view close to the edge of the corral. In some cases, less than a full hemisphere field of view may be adequate, although one usually wants the field of view looking as close as possible to the Sun. In these cases, some illuminated spacecraft appendages or other bright sky objects other than the Sun may acceptably protrude into the field of regard, given that suitable secondary means are then provided that reduce any scattering of this light into the desired field of view down to an acceptable level.

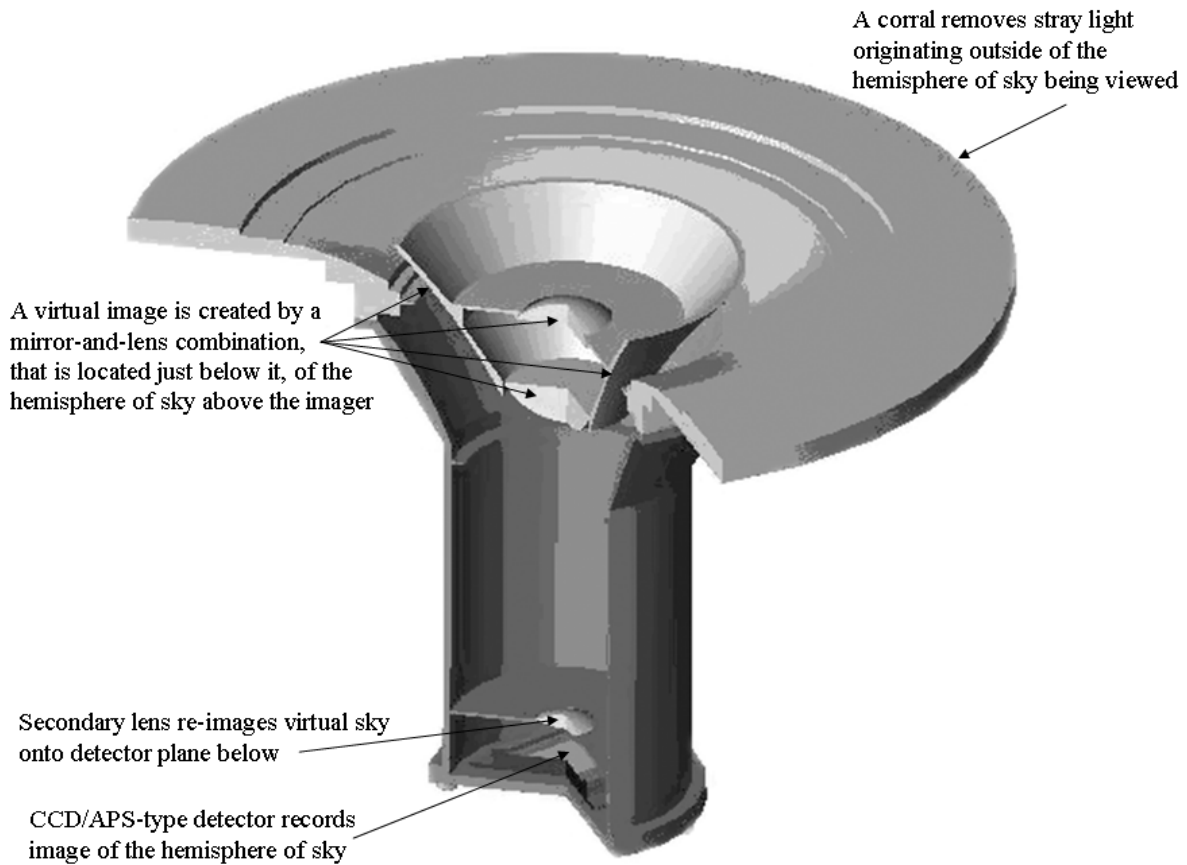


Fig. 1. Cutaway layout of a corral and visible-light optical system covering a hemispherical field of view. The device is suitable for both imaging and precision photometric measurements of heliospheric structures which are made visible by Thomson scattering of sunlight from heliospheric electrons. This lightweight design is also suitable for deployment to deep space (this figure is adapted from Ref. 19).

1.2 Low mass diamond-turned mirror

Most of the hemispherical field of view in this design is provided by the mirror centered in the corral, which covers the sky between 45° and 90° from the optical axis. A major concern is that light from bright objects in or near the field of view that would not normally reach the secondary lens aperture, might scatter into it from the mirror/corral interior, and thus increase stray light reaching the detector. Compared with a conventionally turned and finished mirror, a diamond-turned finish significantly reduces such wide-angle scattering. A hemispherical field of view of the sky inevitably contains bright planets; at L_1 these may include Earth and the Moon. Moreover, the sky within a few degrees of the Sun is much brighter than it is at 90° . When employing sky maps for the 3D reconstructions of heliospheric density and velocity that presently are one of the UCSD main heliospheric analysis products, our experience with bright planets in SMEI has shown that a 10^{-5} scattering surface-brightness reduction in the optics begins to be adequate and that 10^{-6} is quite satisfactory. The diamond-turned mirrors for SMEI were manufactured by some of the present authors.

In order to minimize the mirror mass, the present design removes most material from within it (see figure 2), down to a minimum thickness of 0.2 ± 0.05 cm. Thinner than this, we felt, might cause the interior flange and mounting pads to “show through” to the diamond-turned surface. The resulting final mirror mass is 483.5 gm.



Fig. 2. The lightweight mirror before diamond turning and (for the interior) black anodizing. This size of mirror was chosen to provide 0.1% photometry, within an hour's integration time and a $1^\circ \times 1^\circ$ sky bin, at about 90° elongation from the Sun, at 1 AU.

1.3 Manufacturing details

Inevitably, diamond-turned mirrors that are not “post-polished” retain furrows at the tool-advance spacing; these furrows increase the point-spread-function size, through constructive interference can increase stray-light scattering at certain locations within the field of view, and at large angles through reflection off the tops of the furrows. Post polishing can increase the large-angle scattering, so we have avoided that here. On previous projects the manufacturing of a strongly curved optical surface required motor steps along both X and Y dimensions with the stage moving the tool. This turned out to be extremely demanding for the low-scattering optical surface desired here. Tool motion in both dimensions resulted in small surface non-uniformities compromising wavefront and increasing scattered light. These limitations caused a search for a different approach. To minimize the above defects, the mirror surface here is toroidal, and the diamond-turning tool is mounted so as to move around the generating circle, thus having a “one dimensional motion” as when making a flat mirror. Generating the mirror surface using a smooth curve or radius can improve the surface quality. The challenge here is to diamond-turn a strongly-curved “volcano” shape, and yet retain low-scatter and optically-smooth wavefront.

Turning a lightweight toroid with a nominal 0.2 cm wall thickness, 24 cm base diameter, 8.5 cm height and a 8.9 cm top opening has many challenges. When manufacturing the optical figure one considers the accuracy and material desired. Are the capabilities such that the mounting-fixture tolerances are adequate to retain figure for the duration of the process? Is the material adequate to maintain the figure during the cutting and after release from the mounting fixture? The design of the lightweight substrate and tooling has to be able to maintain optical figure and withstand the cutting forces. The substrate material chosen here is aluminum 6061-T6, QQ-A-225/8, selected free of voids or impurities which could compromise the resulting surface quality. Anodizing the interior surface not only reduces any chance of additional light being scattered. It makes the substrate easy to mount and remount during the process. Therefore the anodizing is done prior to cutting the optical surfaces. The bare aluminum surface is then protected from marks and galling that would otherwise diminish our ability to maintain the tolerances needed. Any stress introduced from the process is then also removed once we turn the optical shape.

Cutting this optic required establishing the radius of the arc along which the cutting tool moves, its center of rotation, and the alignment of the plane of the tool arc. Due to the thin wall, normal mounting or clamping was not feasible or prudent. Several auxiliary fixtures had to be produced to define and include the reference points for the critical location of distance, radius, height and plane. Cutting with a constant speed motor drive starting at the tip of the cone and progressing to the base results in a surface speed change of approximately a ratio 2.3 \times . This required some compromise regarding cutting depth and speed. Experiments with cutting forces and tool position on a similar curve allowed us to choose the best parameters for the final cutting of the optic. The grain direction of the substrate was also considered. The beginning of the cut was near perpendicular to the grain while the ending of the cutting action approached being parallel to the grain.

Once finished the mirror was cleaned with liquid soap and water, rinsed with Isopropyl alcohol and air dried in a clean laminar flow table. Over coating of the mirror with SiO_x was done to protect the Al surface once finished. The optic was rotated about the axis of the cone and positioned such that the source was normal to the center of the arc. Choosing the optimal distance and minimizing the surface’s angular deviation from the source allows for a uniform film thickness, minimizing any change in reflectance over the curved surface.

2. RESULTS

A very qualitative evaluation is provided by simply looking, in bright sunlight, at both the diamond-turned mirror and a conventionally turned one. Figure 3 shows such a comparison. The conventionally-turned-and-polished mirror has a bright line caused by sunlight reflections off the tops of the turning furrows. These are absent from the diamond-turned mirror. Further evaluation of the mirror’s scattering properties takes place within our clean-room HEPA-filtered workstation (figures 4 and 5). The beam from a Neon-Helium laser illuminates the mirror, and the brightness of the spot upon it evaluated using neutral-density filters and, with care, the eye as a photometer. The spot is seen to have a component of near-Lambertian scattered light at $\sim 1/3$ the surface brightness of Martin Black²⁰, when a sample of the latter is placed in the laser beam just before the mirror. Our prior experience with this black surface²¹ indicates that here about 10^{-3} of the incident light enters this Lambertian component. Its brightness changes little with illumination location on the mirror and incident angle. The spot visibly brightens when one’s viewing angle approaches the direction for specular reflection; it is $\sim 3\times$ and $10\times$ brighter respectively at scattering angles of 20° and 10° than it is at large angles.

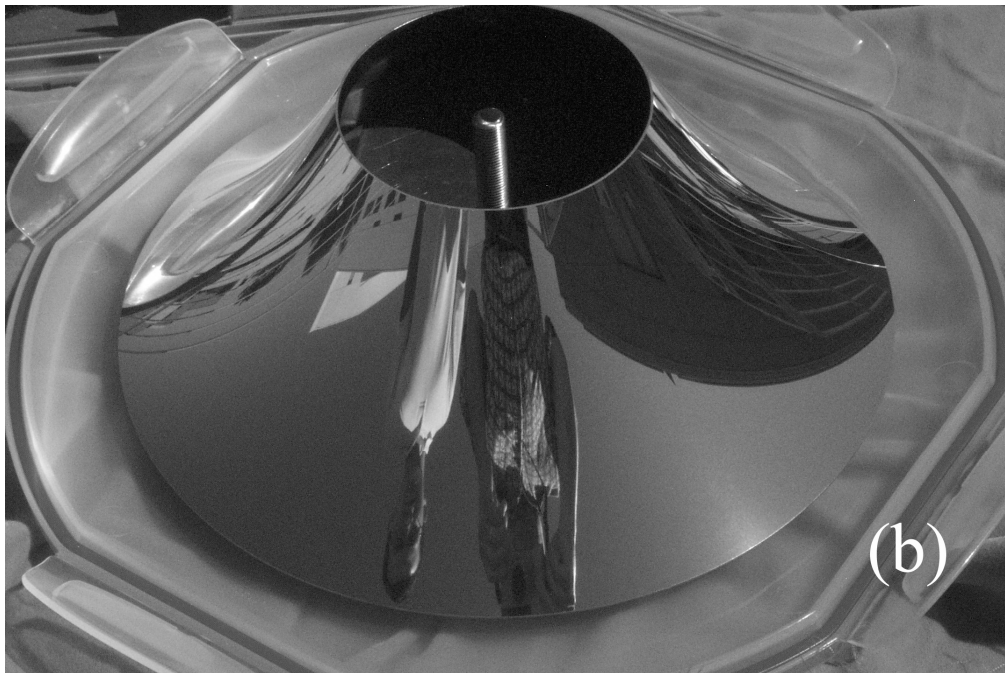
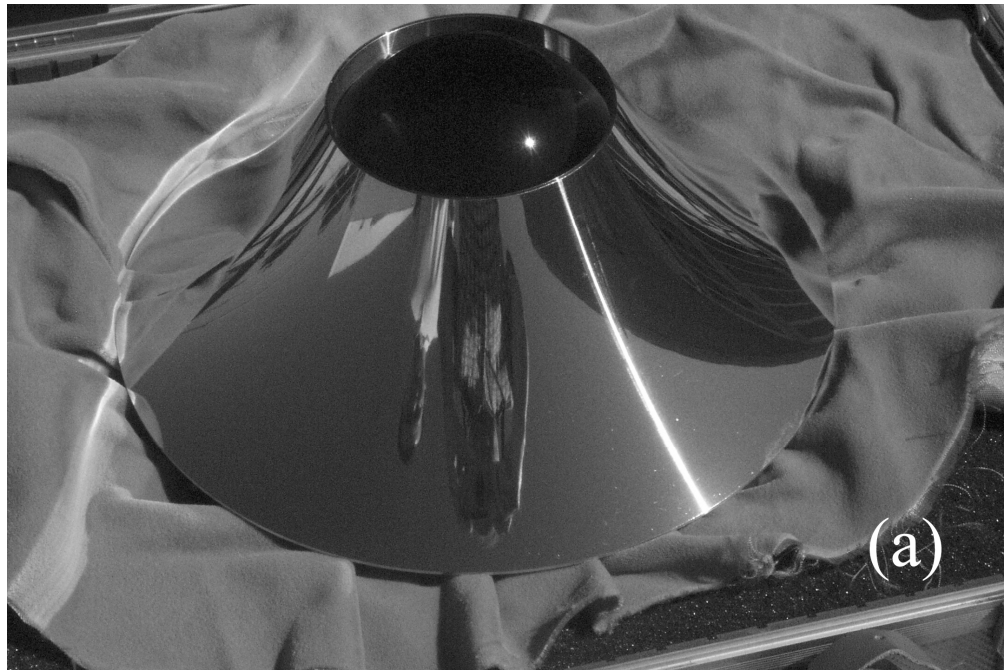


Fig. 3. (a) Conventionally turned mirror for a visible-light hemispherical optical system¹⁶ (and also presented upon the cover of that issue of *Applied Optics*). Here, and in (b), the reflection of the Sun is placed just off the mirror to the bottom right. (b) Same configuration and photographic exposure, but for the diamond-turned mirror. The prominent reflected-Sun bright line in (a) is visibly absent in (b).

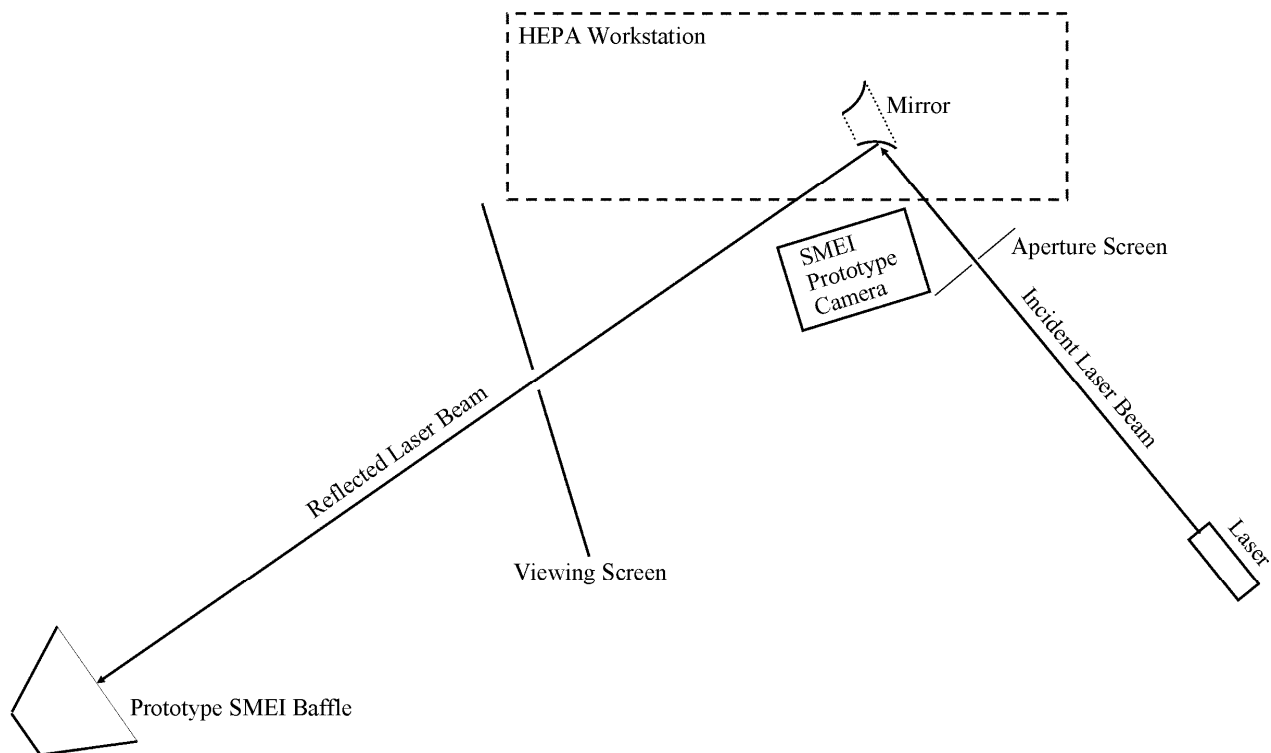


Fig. 4. Schematic plan diagram of the stray-light measurement setup within the UCSD clean room. The mirror being tested remains within the HEPA Workstation and is illuminated as shown by a laser beam. The Aperture Screen removes laser light outside of the main beam. Specular-reflected light passes through a hole in the Viewing Screen and is absorbed into the SMEI Prototype Baffle. Stray-light scattering by the mirror illuminates the viewing screen, where it is recorded by the SMEI Prototype Camera (§ 2.2), or by a smaller digital camera placed immediately in front of it (§ 2.1).

2.1 Scattered-light photographic measurements

A more quantitative evaluation of scattered light is provided by measurements utilizing our setup as shown in figures 4 and 5. Here the contribution to scattered light is small from dust particles in the air, and the diamond-turned mirror can be left for weeks within the work station without picking up significant contamination. We first present results using a digital camera. This is advantageous because in a single image it presents a qualitative evaluation of stray light scattered by 2° to 20° from the specular-reflected beam. Our photometric camera (next section) provides the best quantitative scattering results, but over a more-restricted field of view.



Fig. 5. Photograph of the clean room setup used for the measurements presented here. A specular-reflected laser beam is drawn in to highlight the light's path. Light scattered by more than about 2° , out to about 20° becomes visible on the white paper placed upon the Viewing Screen, where it can then be photographed by a conventional digital camera or photometrically recorded using the SMEI Prototype Camera.

The hole in the Viewing Screen was covered with white paper, and the specular-reflected light pattern photographed with a Canon PowerShot G10 digital camera. This is shown in figure 6(a). The scattered-light pattern with the hole open is shown in figure 6(b). For these, the laser spot was placed about halfway between the mirror's wide base and narrow opening. To extract qualitative brightness information from figure 6, we have used a photo-editing program to determine fractional brightness relative to "full scale", the maximum reading in the picture's 8-bit digitized result. In (a), peak brightness is ~ 0.8 and roughly 45,000 pixels are above 0.4. Thus, were all the specular-reflected light in (a) to be combined into one pixel, its brightness reading would be 3.6×10^4 . Differing exposure times introduce a factor of 3750 between (a) and (b), so scaling this number to (b) yields 1.35×10^8 . In (b) at the edge of the viewing screen, a $\sim 20^\circ$ scattering angle, the brightness per pixel above background is about 0.05 of full scale. Thus the ratio in brightness of a single pixel at this angle to the surface brightness at the center of the specular-reflected spot in (a) is about 3.7×10^{-10} .

Scattered-light surface brightness increases towards smaller scattering angles nearer the center of the screen. At a scattering angle of 4° (about twice the radius of the hole), the increase is $\sim 5\times$ for scattering parallel to the furrow direction and $\sim 10\times$ for scattering perpendicular to the furrow direction (respectively, the vertical and horizontal axes in fig.6(b)). A residue of interference fringes from the turning furrows is barely visible as short vertical lines distributed along a horizontal line in the middle of the picture.

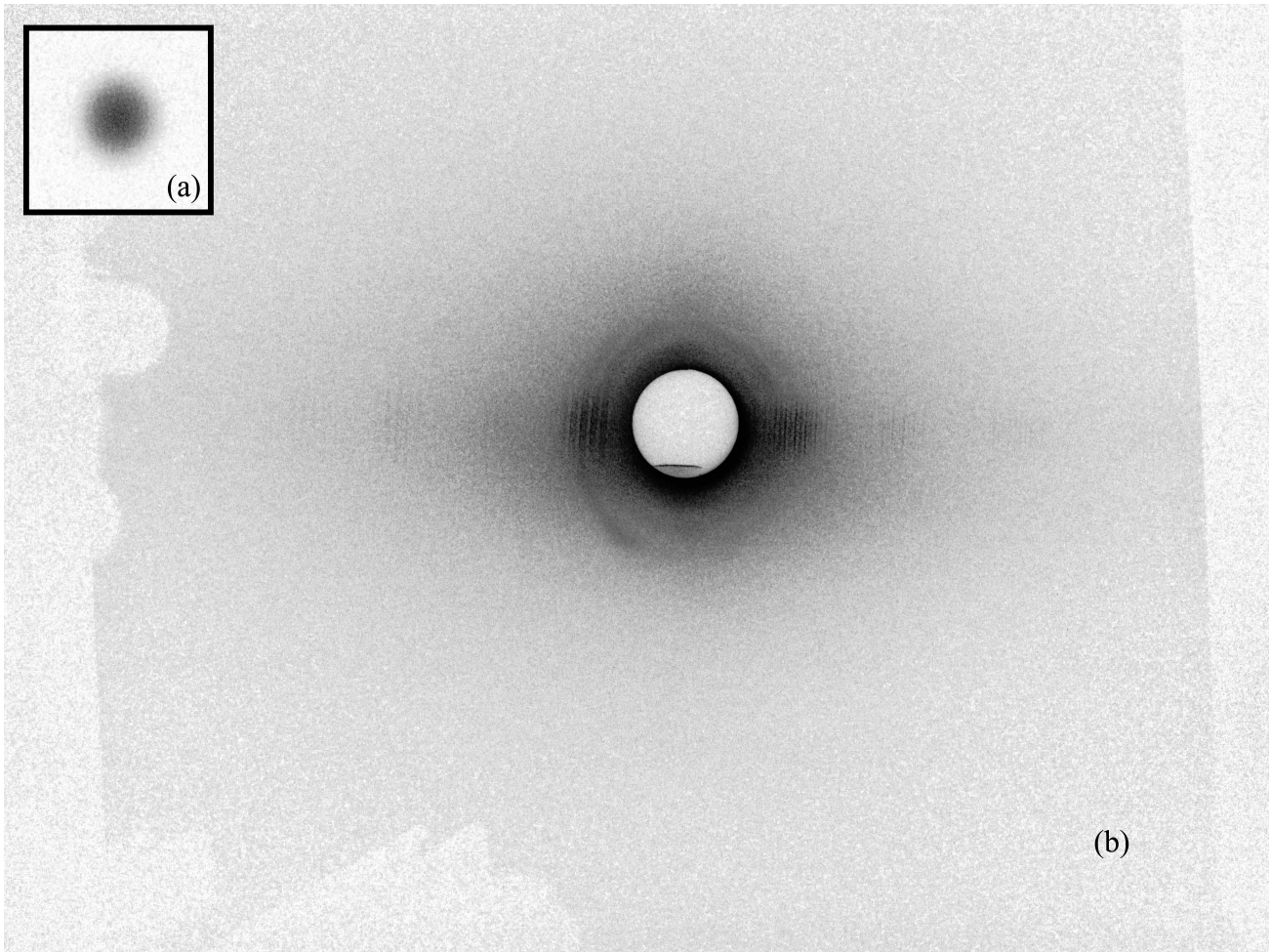


Fig. 6. Reflected light on the viewing screen as recorded by digital camera, with settings $f/2.8$ and ISO1600. Here the gray scale goes from zero (white) to full brightness (black). (a) The specular reflected spot on white paper (filling the hole) and a $1/250$ sec exposure. (b) The hole open as in fig. 4, and a 15 sec exposure. Here the direction of scatter parallel to the diamond-turning furrow direction is roughly vertical, perpendicular is horizontal, and the scattering angles between the main spot (center of the hole) and the left- and right-hand edges of the viewing screen are about 18° and 22° respectively. Faint rings roughly concentric with the hole and of about twice its radius are artifacts of diffraction by the opening in the aperture screen. In (b) a background (of light from the screen going out into the room and re-scattering back onto the screen from objects there) about 0.07 of full brightness, is visible right and left beyond the edge of the viewing screen. The irregular boundary near the edge of the picture below left is caused by shadowing by the SMEI vacuum tank's mounting rails, and the round shadows toward the left edge by the tank's plumbing valves.

2.2 Scattered-light photometric measurements

The SMEI Prototype Camera provides our best quantitative results; it was used to certify the 0.1% photometric capabilities of the SMEI optics and CCD detector. Its surface-brightness measurements are in analog-to-digital units (ADUs) with a 14-bit useable dynamic range¹. Its $60^\circ \times 3^\circ$ field of view (FOV) records stray-light scattering along selected strips of the picture in fig. 6. Let Θ_\perp and Θ_\parallel respectively denote scattering angle perpendicular and parallel to the diamond-turning furrow direction. For the data presented here, the SMEI camera is oriented to measure light scattered along one of these while the other is zero. In fig. 5 horizontal is scattering along Θ_\perp and vertical is along Θ_\parallel . To reduce background light, the white screen shown in fig. 5 is removed, and smaller sheets of white paper are pinned to

the screen in the desired locations, to be illuminated by either specular reflected light (figs. 7(a) and 7(c)) or scattered light (figs. 7(b) and 7(d)) from the diamond-turned mirror. A background, which typically has a surface brightness of around 10 ADUs, is light from the illuminated paper that has been re-scattered back onto the paper from objects within the room. For results here, data recorded by the camera have pedestal and dark current removed, individual-pixel readings are corrected for the different solid angles subtended by each and for the aperture's projected area, and finally an estimate of the background is subtracted.

Figures 8 and 9 show the ADUs averaged over a 1° wide band running along each case in fig. 7. Angle is here converted from the SMEI camera viewing angle to scattering angle at the diamond-turned mirror. The beam total is $\sim 7 \times 10^7$ ADUs, and thus a scattering probability $d^2P/d\Theta_{\parallel}d\Theta_{\perp}$ per square degree, at a given angle Θ_{\perp} (fig. 8) or Θ_{\parallel} (fig. 9), is given by dividing the observation by this total. In fig. 8, the roughly exponential dropoff beginning at about $\pm 8^\circ$ presumably flattens off to a value of about 10^{-7} on the right-hand scale, not far beyond the $\pm 20^\circ$ range of data in this plot, to properly join onto the Lambertian large-angle component described previously. In fig. 9, the exponential dropoff is already close to this value and probably does not become much smaller at larger scattering angles.

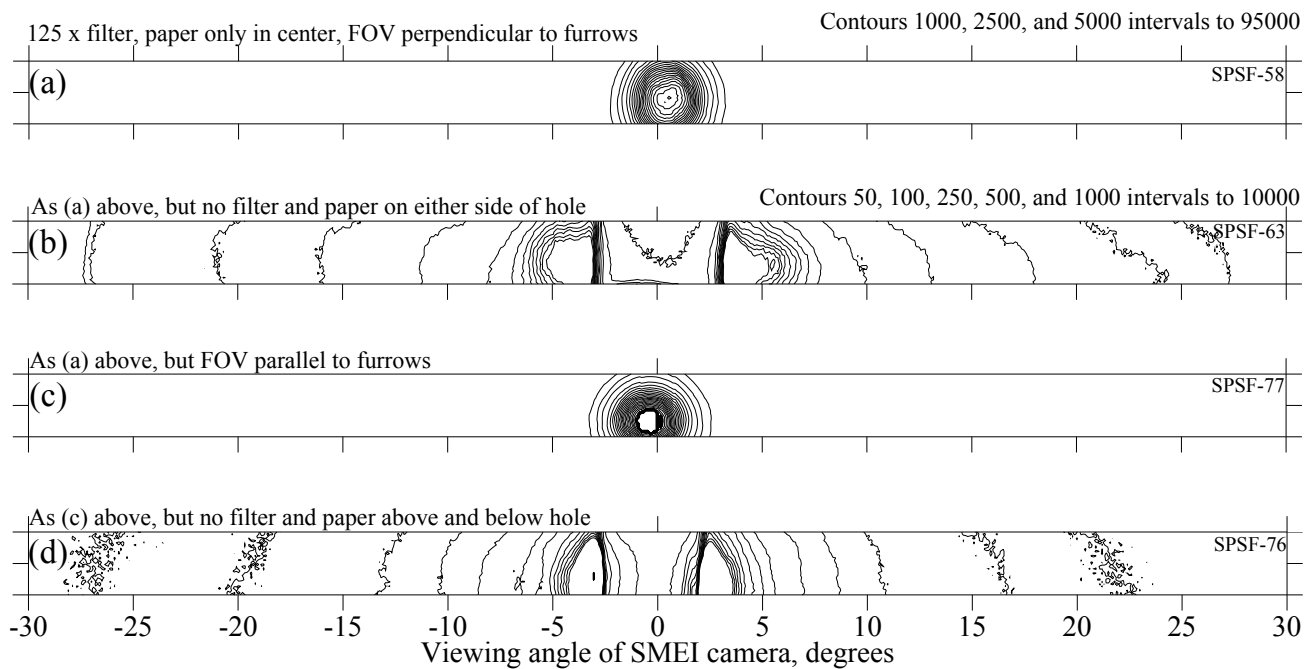


Fig. 7. The photometric readings making up the results presented here, surface brightness as recorded by the SMEI camera. The field of view (FOV) is 60° wide by 3° high and the x -axis here labels angle as viewed from the SMEI aperture along the 60° direction. The exposure time is 1 sec. For panels (a) and (c) a $125\times$ neutral-density filter reduces the brightness of the main spot illuminating the white paper which in this case is covering the slot in the Viewing Screen. For Panels (b) and (d) the light from the main spot passes through the slot in the Viewing Screen and is absorbed in the SMEI Prototype Baffle.

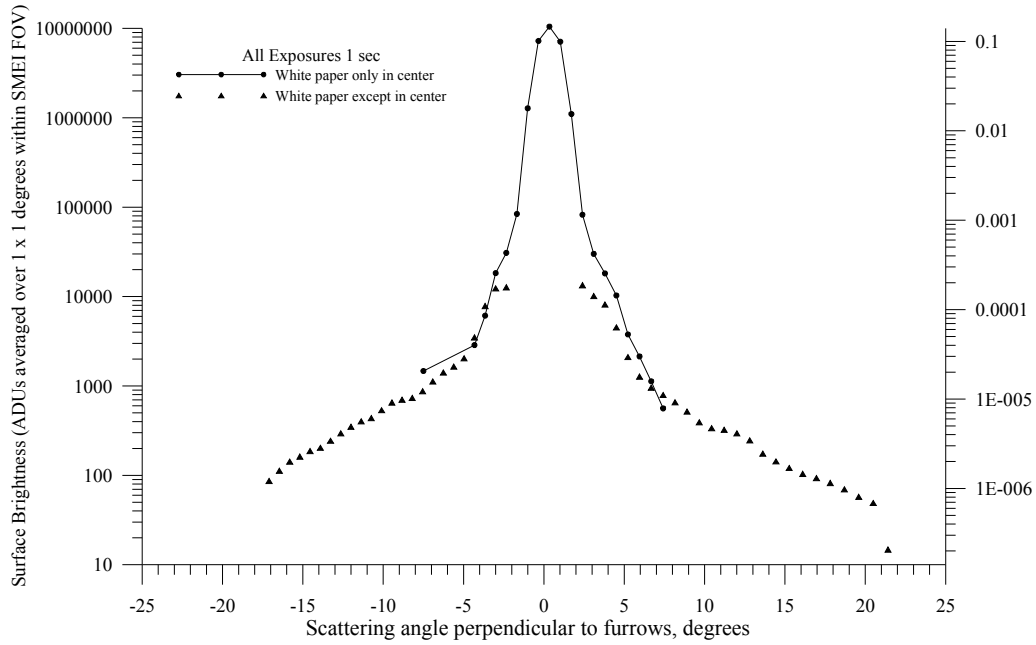


Fig. 8. Surface brightness versus Θ_{\perp} (scattering angle perpendicular to the furrow direction) at $\Theta_{\parallel} = 0$. Data for the white paper in center (circles) are increased by $125\times$, to correct for the neutral-density filters used to keep the bright spot within the SMEI camera's dynamic range. The right-hand scale shows the scaled $d^2P/d\Theta_{\parallel}d\Theta_{\perp}$ along $\Theta_{\parallel} = 0$ that results from dividing the left-hand scale by 7×10^7 , total brightness contained in the central peak.

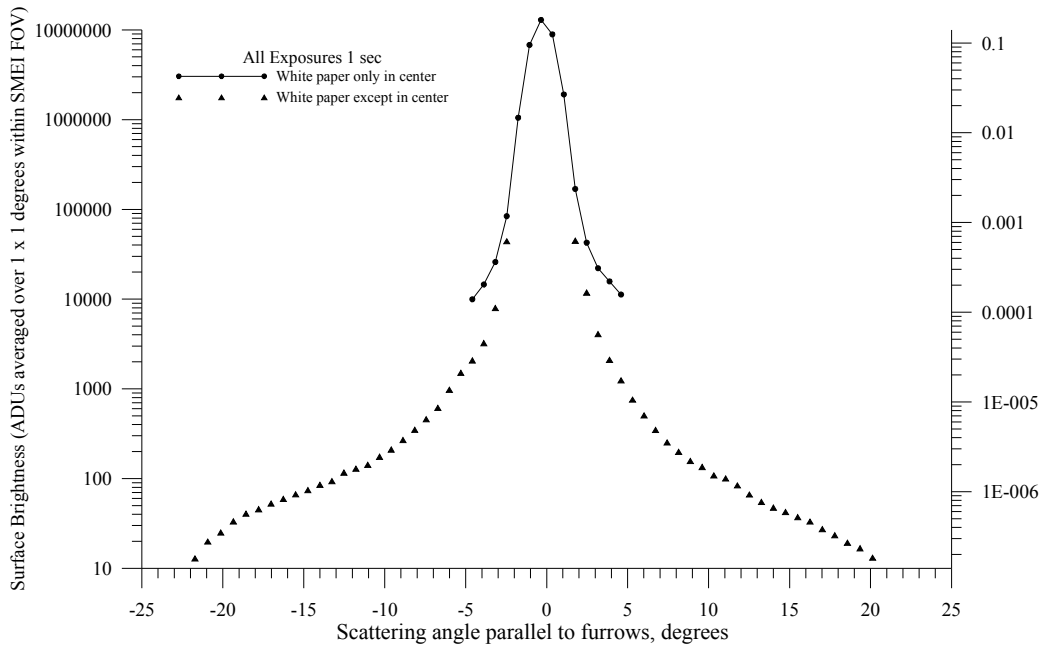


Fig. 9. Surface brightness versus Θ_{\parallel} (scattering angle parallel to the furrow direction) at $\Theta_{\perp} = 0$. Data for the white paper in center (circles) are increased by $125\times$, to correct for the neutral-density filters used to keep the bright spot within the SMEI camera's dynamic range. As with fig. 8, the right-hand scale shows the scaled $d^2P/d\Theta_{\parallel}d\Theta_{\perp}$ along $\Theta_{\perp} = 0$ that results from dividing the left-hand scale by 7×10^7 .

3. SUMMARY AND DISCUSSION

Figs. 8 and 9 directly measure scattering from this strongly-curved diamond-turned mirror. Although the aperture screen removes most of the laser beam's off-axis light beyond 1° to 2° , some contamination persists out to about 4° . Beyond this, $d^2P/d\Theta_{\parallel}d\Theta_{\perp}$ diminishes roughly exponentially both along $\Theta_{\parallel} = 0$ and along $\Theta_{\perp} = 0$, with a $1/e$ characteristic angle of about 4° . Extrapolating these exponentials back to zero angle yields $d^2P/d\Theta_{\parallel}d\Theta_{\perp}$ intercepts of about 4×10^{-5} and 1×10^{-5} respectively for Θ_{\perp} and Θ_{\parallel} . The present measurements extend out to scattering angles of about 20° . Beyond this, the exponentials presumably both level off to assume a constant value near 10^{-7} , the very wide-angle Lambertian component determined here by comparing the illuminated-spot brightness on the mirror with that on a Martin Black sample. Little evidence is seen here of constructive-interference scattering that might be present because of the periodic structure of diamond-turning furrows.

The present measurements are preliminary. A more complete investigation will: (1) reduce the re-scattered background light which was estimated and then subtracted here; (2) reduce the laser-beam off-axis contamination and thus extend the direct scattering measurements to cover angles between 1° and 4° ; and finally (3) extend the measurements beyond 20° .

A principal accomplishment here for a strongly-curved mirror, is the reduction of wide-angle scattering down to that typical of a diamond-turned flat mirror. For good photometric measurements of the heliosphere, keeping a distance of several degrees away from bright planets will still be required as it is for SMEI, but the present manufacturing process cures the bright line reaching out much further than this, as seen in fig. 3(a) and also is seen in SMEI results. Another accomplishment is the successful manufacturing and testing of a lightweight mirror practical for use as a heliospheric imager to be deployed at ~ 1 AU. For missions closer to the Sun, a smaller and even more lightweight mirror would likely be appropriate.

Finally we note that SMEI provides a spaceborne antecedent for similar diamond-turned mirrors that have performed well in space, and that a similarly-made flat mirror employed by the imager on STARDUST²² produced very good results from deep space²³.

ACKNOWLEDGEMENTS

We at UCSD thank Philippe Leblanc for his careful mirror-design work, Ed Stephan for his continuing interest and support, and John Clover and Sally Buffington for useful suggestions regarding the manuscript. This work was supported in part by NASA #NNX08AJ11G and by U.S. Air Force #FA9550-06-1-0107. Manufacturing the low-mass mirror evaluated here was supported by Contract #NAS2-03145 at the NASA/Ames Research Center.

REFERENCES

- [1] Eyles, C.J., Simnett, G.M., Cooke, M.P., Jackson, B.V., Buffington, A. and Hick, P.P., Waltham, N.R., King, J.M., Anderson, P.A. and Holladay, P.E., 'The Solar Mass Ejection Imager (SMEI)', *Solar Phys.* **217**, 319-347, 2003.
- [2] Jackson, B.V., Buffington, A., Hick, P.P., Altrock, R.C., Figueroa, S., Holladay, P.E., Johnston, J.C., Kahler, S.W., Mozer, J.B., Price, S., Radick, R.R., Sagalyn, R., Sinclair, D., Simnett, G.M., Eyles, C.J., Cooke, M.P., Tappin, S.J., Kuchar, T., Mizuno, D., Webb, D.F., Anderson, P.A., Keil, S.L., Gold, R.E. and Waltham, N.R., 'The Solar Mass Ejection Imager (SMEI) Mission', *Solar Phys.* **225**, 177-207, 2004.
- [3] Tappin, S.J., and 16 co-authors, 'Tracking a major interplanetary disturbance with SMEI', *Geophys. Res. Lett.* **31**, L2802-L2805, 2004.
- [4] Webb, D.F., Mizuno, D.R., Buffington, A., Cooke, M.P., Eyles, C.J., Fry, C.D., Gentile, L.C., Hick, P.P., Holladay, P.E., Howard, T.A., Hewitt, J.G., Jackson, B.V., Johnston, J.C., Kuchar, T.A., Mozer, J.B., Price, S., Radick, R.R., Simnett, G.M. and Tappin, S.J., 'Solar Mass Ejection Imager (SMEI) Observations of CMEs in the Heliosphere', *J. Geophys. Res.* **111**, A12101, 2006.

- [5] Howard, T.A., Webb, D.F., Tappin, S.J., Mizuno, D.R. and Johnston, J.C., 'Tracking halo coronal mass ejections from 0-1 AU and space weather forecasting using the Solar Mass Ejection Imager', *J. Geophys. Res.* **111**, A04105, 2006.
- [6] Mizuno, D. R., Buffington, A., Cooke, M. P., Eyles, C. J., Hick, P. P., Holladay, P. E., Jackson, B. V., Johnston, J. C., Kuchar, T. A., Mozer, J. M., Price, S. D., Radick, R. R., Simnett, G. M., Sinclair, D. and Webb, D. F. 'Very High-Altitude Aurora Observations With The Solar Mass Ejection Imager', *J. Geophys. Res.* **110**, 7230-7247, 2005.
- [7] Kuchar, T.A., Buffington, A., Howard, T.A., Arge, C.N., Hick, P.P., Jackson, B.V., and Webb, D.F., 'The Evolution of Comets in the Heliosphere as Observed by SMEI', *EOS Trans. AGU*, **87** (52), Fall Meet. Suppl. Abstr. SH32A-08, 2006.
- [8] Kuchar, T.A., Buffington, A., Arge, C.N., Hick, P.P., Howard, T.A., Jackson, B.V., Johnston, J.C., Mizuno, D.R., Tappin, S.J., and Webb, D.F., 'Observations of a Comet Tail Disconnection Induced by CME Passage', *J. Geophys. Res.*, **113**, A04101, doi:10.1029/2007JA012603, 2008.
- [9] Buffington A., Bisi, M.M., Clover, J.M., Hick, P.P., Jackson, B.V., and Kuchar, T.A., 'Analysis of Plasma-Tail Motions for Comets C/2001 Q4 (NEAT) and C/2002 T7 (LINEAR) using Observations from SMEI', *Astrophys. J.*, **677**, 798-807, 2008.
- [10] Buffington, A., Bisi, M. M., Clover, J. M., Hick, P. P., Jackson, B. V., Kuchar, T. A., and Price, S. D. 'Measurements of the Gegenschein brightness from the Solar Mass Ejection Imager (SMEI)', *Icarus* (in press), doi:10.1016/j.icarus.2009.04.007, 2009.
- [11] Jackson, B. V., Buffington, A., Hick, P.P., Wang, X. and Webb, D., 'Preliminary three-dimensional analysis of the heliospheric response to the 28 October 2003 CME using SMEI white-light observations', *J. Geophys. Res.* **111**, A4, A04S91, 2006.
- [12] Jackson, B. V., Bisi, M. M., Hick, P. P., Buffington, A., Clover, J. M., and Sun, W. 'Solar Mass Ejection Imager (SMEI) 3D reconstruction of the 27-28 May 2003 CME sequence', *J. Geophys. Res.*, **113**, A00A15, doi:10.1029/2008JA013224, 2008.
- [13] Jackson, B.V., Buffington, A., Hick, P.P., Bisi, M.M., and Jensen, E.A. 'SMEI Observations in the STEREO Era', *Proc. SPIE* **6689**, 66890G, 2007.
- [14] Bisi, M. M., Jackson, B. V., Hick, P. P., Buffington, A., Odstrcil, D., and Clover, J. M. '3D Reconstructions of the Early-November 2004 CDAW Geomagnetic Storms: Analyses of STELab IPS Speed and SMEI Density Data', *J. Geophys. Res.*, **113**, A00A11, doi:10.1029/2008JA013222, 2008.
- [15] Buffington, A., Hick, P.P., Jackson, B.V., and Korendyke, C.M., 'Corrals, hubcaps, and crystal balls: some new designs for very-wide-angle visible-light heliospheric imagers', *Proc. SPIE* **3442**, 77-86, 1998.
- [16] Buffington, A., 'Very-wide-angle optical systems suitable for a spaceborne optical hemispherical imager', *Applied Optics* **39**, 4284-4293, 2000.
- [17] Buffington, A., 'Improved design for stray-light reduction with a hemispherical imager', *Appl. Optics* **39**, 2683-2686, 2000.
- [18] Jackson, B.V., Buffington, A., and Hick, P.P., 'A heliospheric imager for Solar Orbiter', Proceedings of Solar Encounter: The First Solar Orbiter Workshop, Puerto de la Cruz, Tenerife, Spain 14 -18 May 2001, (ESA SP-493, September 2001), 251-254, 2001.
- [19] Jackson, B.V., 'PERSEUS Mission: Investigating global heliospheric dynamics from L₁', proposal submitted from UCSD in response to NASA NRA NNH07ZDA003O, 2008.
- [20] 'Optical black coating', Martin Marietta Company, *Proc. SPIE* **107**, 168-169, 1977.
- [21] Buffington, A., Jackson, B.V., and Hick, P.P., 'Calculations for, and laboratory measurements of a multistage labyrinthine baffle for SMEI', *Proc. SPIE* **4853**, 490-503, 2003.
- [22] Newburn, R.L., Bhaskaran, S., Duxbury, T.C., Frascchetti, G., Radey, T., and Schwochert, M., 'Stardust Imaging Camera', *J. Geophys. Res.*, **108**, NO. E10, 8116, doi:10.1029/2003JE002081, 2003.
- [23] Tsou, P., and 19 co-authors, 'Stardust encounters comet 81P/Wild 2', *J. Geophys. Res.*, **109**, E12S01, doi:10.1029/2004JE002317, 2004.